RSC Advances

PAPER

View Article Online
View Journal | View Issue



Cite this: *RSC Adv.*, 2021, **11**, 7214

# Catalytically active nanosized $Pd_9Te_4$ (telluropalladinite) and PdTe (kotulskite) alloys: first precursor-architecture controlled synthesis using palladium complexes of organotellurium compounds as single source precursors†

Aayushi Arora,[a] Preeti Oswal,[a] Gyandshwar K. Rao,[b] Sushil Kumar,[a] Ajai K. Singh[c] and Arun Kumar*[a]

Received 13th October 2020
Accepted 7th January 2021

DOI: 10.1039/d0ra08732g

rsc.li/rsc-advances

Several intermetallic binary phases of Pd–Te including $Pd_3Te_2$, PdTe, $PdTe_2$, $Pd_9Te_4$, $Pd_3Te$, $Pd_2Te$, $Pd_{20}Te_7$, $Pd_8Te_3$, $Pd_7Te_2$, $Pd_7Te_3$, $Pd_4Te$ and $Pd_{17}Te_4$ are known, and negligible work (except few studies on PdTe) has been done on exploring applications of such phases and their fabrication at nanoscale. Hence, Pd(II) complexes Pd(**L1**)$Cl_2$ and Pd(**L2**-H)Cl (**L1**): Ph–Te–$CH_2$–$CH_2$–$NH_2$ and **L2**: HO–2-$C_6H_4$–CH=N–$CH_2CH_2$–Te–Ph were synthesized. Under similar thermolytic conditions, complex Pd(**L1**)$Cl_2$ with bidentate coordination mode of ligand provided nanostructures of $Pd_9Te_4$ (telluropalladinite) whereas Pd(**L2**-H)Cl with tridentate coordination mode of ligand yielded PdTe (kotulskite). Bimetallic alloy nanostructures possess high catalytic potential for Suzuki coupling of aryl chlorides, and reduction of 4-nitrophenol. They are also recyclable upto six reaction cycles in Suzuki coupling.

## Introduction

Materials at nanoscale possess new and improved properties compared to their bulk counterparts. Hence, the scientific community has focused its attention on the fabrication of nano-sized materials.[1] Composition, stability, size and shape are among those factors on which the physicochemical properties of nanomaterials have been found to depend.[1] In this regard, metal chalcogenide nanomaterials[1–3] have attracted the attention of researchers increasingly due to their various applications in energy conversion, storage and electronics,[2–5] development of materials for semiconductors,[6–8] dye-sensitized solar cells,[9,10] magnesium–air batteries,[11] aerogel fabrication,[12] and catalysis.[13–20]

Among different metal chalcogenides reported in literature, significant work has been done in recent past on the exploration and development of binary phases of tellurides of various metals (excluding palladium), mainly due to their potential application[2] in memory devices, photovoltaic cells, thermoelectrics, biochemical applications, semiconductors with enhanced thermoelectric properties in nanocomposites, photothermal therapy, thin films and nanomaterials and catalysis.[2,4,18–20] After the discovery of easy methods of preparation[16,17,21] of binary phases of palladium selenide and their role in catalysis,[16,17] there has been an enormous increase during last five years on the discovery of interesting applications of palladium selenides[3,9–14] in various fields including catalysis. Binary phases of palladium tellurides are also envisaged to be among applied nanomaterials. Binary phases reported so far include PdTe, $Pd_3Te_2$, $PdTe_2$, $Pd_9Te_4$, $Pd_{2.5}Te$, $Pd_3Te$, $Pd_2Te$, $Pd_{20}Te_7$, $Pd_8Te_3$, $Pd_7Te_2$, $Pd_7Te_3$, $Pd_4Te$ and $Pd_{17}Te_4$.[22] Among such phases, only PdTe,[18–20] $Pd_{20}Te_{27}$ (ref. 23) and $Pd_{13}Te_3$ (ref. 24) have been studied upto some extent. Catalysis, an important applications of other metal chalcogenides, has not seen the potential of binary phases of palladium tellurides except a few reports on PdTe.[18–20]

$Pd_9Te_4$ (telluropalladinite), an intermetallic system, is a palladium rich binary phase which was reported by Matkovic and Schubert for the first time in year 1978.[25] Only a little is known and reported about this material.[25,26] Its crystal structure[25] and phase relations[26] has been studied. To the best of our knowledge, laboratory synthesis for its bulk material is rarely investigated, and its fabrication at nanoscale and potential applications have not yet been investigated.

A convenient route to produce metal chalcogenide materials is by thermal decomposition[6,7] of single source precursors (SSP) *i.e.* metal complexes containing organochalcogen ligands. This

[a]Department of Chemistry, School of Physical Sciences, Doon University, Dehradun, Uttarakhand, 248012, India. E-mail: arunkaushik@gmail.com; akumar.ch@doonuniversity.ac.in

[b]Department of Chemistry, Amity School of Applied Sciences, Amity University Haryana (AUH), Gurgaon, Haryana, 122413, India

[c]Department of Chemistry, Indian Institute of Technology Delhi, New Delhi, 110016, India

† Electronic supplementary information (ESI) available. CCDC 1994615 and 1994616. For ESI and crystallographic data in CIF or other electronic format see DOI: 10.1039/d0ra08732g

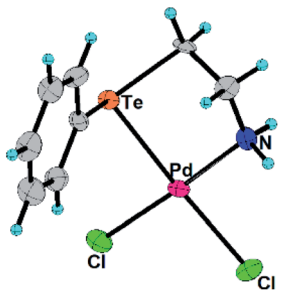


Fig. 1 ORTEP diagram of complex **1** with 50% thermal ellipsoids. Selected bond lengths (Å): Te–Pd: 2.5057(6), Te–$C_{aryl}$: 2.118(6), Te–$C_{alkyl}$: 2.149(6), Pd–Cl: 2.3142(16), Pd–Cl; Pd–N: 2.063(5). Selected bond angles (°): Cl–Pd–Te: 88.82(4), Cl–Pd–Cl: 94.42(6), N–Pd–Te: 88.21(13), N–Pd–Cl: 88.54(14).

route has advantages over the conventional methods as it does not require distinct sources for palladium and chalcogen, sophisticated equipments and extremely high temperature. Since molecules of only a single precursor are available in the reaction vessel in SSP route, reaction handling becomes easy and the possibility of occurrence of pre-reaction and contamination is minimized. The work-up procedures are also simple due to easy removal of organic by-products by filtration or centrifugation. Some metal complexes (except those of Pd and Pt) of tellurium ligands have been used as SSPs for the synthesis of nanosized binary tellurides (such as $Sb_3Te_2$, SnTe, PbTe, ZnTe and CdTe) of different metals.[2,6,8] Though the ligand chemistry of organotellurium compounds is explicitly explored with palladium and a variety of coordination compounds have been synthesised,[6,8] use of such compounds as SSPs for the development of nanostructures of binary phases of palladium tellurides at bulk or nano-scale have been rarely explored.[24] However, *in situ* generation of $Pd_3Te_2$ nanoparticles has been reported during catalysis of a Suzuki–Miyaura coupling by a tellurium ligated molecular Pd(II) complex.

It is worth noting that (i) a little has been studied and reported about most of the binary phases of palladium tellurides including $Pd_9Te_4$ which has not been fabricated at nanoscale so far and not explored for applications, (ii) there are only a few reports on the synthesis of PdTe nanocrystals, (iii) molecular architecture of precursor plays a significant role in determining the composition and/or morphology of nanostructures in SSP route,[1,17,27] (iv) applications of binary phases of palladium tellurides are rarely explored in catalysis, and (v) when dispersion of nano-scale palladium tellurides continues to decrease and reaches the single atom limit, it may become a single-atom catalyst. Such single atom catalysts are expected to obtain better catalytic activity and efficiency.[28–31] It is, therefore, thought to develop a SSP based easy route for the precursor-architecture controlled synthesis of PdTe and $Pd_9Te_4$ nanostructures, and to carry out the screening of their catalytic potential for Suzuki coupling of chloroarenes and reduction of 4-nitrophenol, the chemical transformations of immense utilities.[32,33]

In the present work, the ligands **L1**, **L2** and their Pd(II) complexes **1** and **2** have been synthesized. The major structural difference between **1** and **2** is the coordination mode (Fig. 1 and 2) of ligand (*i.e.* bidentate in **1** and tridentate in **2**). The **1** and **2** have been used as designers single source precursors to obtain nanoparticles of different alloys ($Pd_9Te_4$ from **1** and PdTe from **2**) under similar conditions of thermolysis. Both the nanosized alloys show a high potential for catalysis of Suzuki coupling and reduction of nitroarenes.

As an enormous surge in the investigations on interesting applications of binary phases (such as $Pd_{17}Se_{15}$, $Pd_4Se$ and $Pd_7Se_4$) of palladium selenide has been noticed after year 2015,[3,9–14] the results of this report open up a field for development of

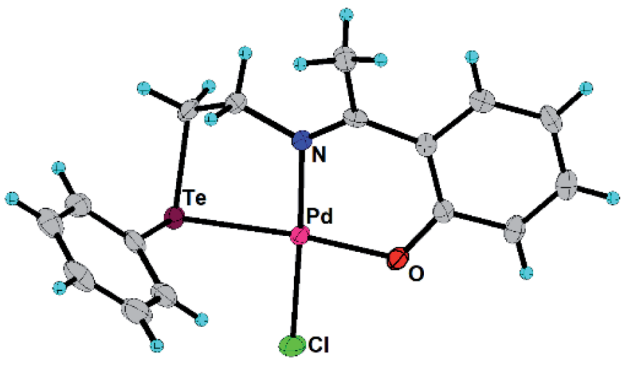


Fig. 2 ORTEP diagram of complex **2** with 50% thermal ellipsoids. Selected bond lengths (Å): Te–Pd: 2.5002(4), Te–C: 2.120(4), Pd–Cl: 2.3271(11), Pd–O: 2.007(3), Pd–N: 2.017(4). Selected bond angles (°): Cl–Pd–Te: 86.74(3), O–Pd–Cl: 88.98(9), N–Pd–Te: 90.94(10), N–Pd–O: 93.18(13).

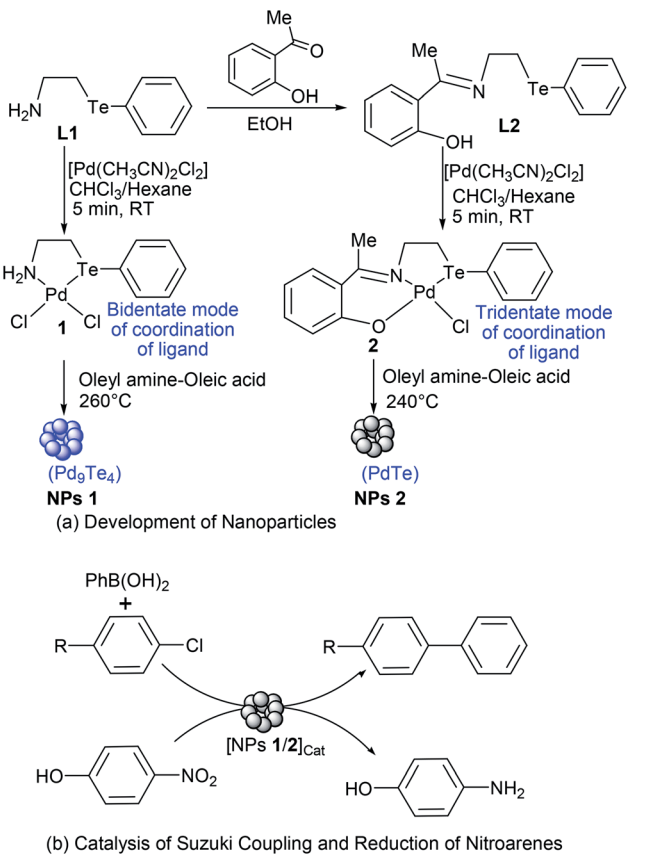


Scheme 1 Strategy for syntheses and catalytic reactions.

Table 1 Crystal data and structural refinement parameters of complexes **1** and **2**

| Parameters | 1 | 2 |
|---|---|---|
| Formula | $C_8H_{11}Cl_2NPdTe$ | $C_{16}H_{16}ClNOPdTe$ |
| Formula weight (g mol$^{-1}$) | 426.08 | 507.75 |
| Color | Yellow | Orange |
| Space group | $P1$ | $P2_1/n$ |
| Temperature/K | 293(2) | 150.00(10) |
| $\lambda$ (Å) (Cu-K$\alpha$) | 0.71073 | 0.71073 |
| Crystal system | Triclinic | Monoclinic |
| $a$ (Å) | 7.9097(8) | 16.7218(2) |
| $b$ (Å) | 8.4514(10) | 19.2440(3) |
| $c$ (Å) | 8.85568(7) | 20.2510(3) |
| $\alpha$ (°) | 83.934(8) | 90 |
| $\beta$ (°) | 87.438(8) | 99.6590(10) |
| $\gamma$ (°) | 86.644(9) | 90 |
| $V$ (Å$^3$) | 567.27(10) | 6424.28 |
| $Z$ | 2 | 16 |
| $\rho_{calc}$ (g cm$^{-3}$) | 1.083 | 2.099 |
| $F(000)$ | 396 | 3872 |
| Theta range for data collection | $2.395 < \theta < 28.123$ | $2.0240 < \theta < 28.0940$ |
| Index ranges | $-8 < h < 10$ | $-21 < h < 22$ |
| | $-11 < k < 10$ | $-24 < k < 25$ |
| | $-9 < l < 11$ | $-11 < l < 27$ |
| GOF on $F^2$ | 1.059 | 1.0263 |
| $R1$ [$I > 2\sigma(I)$] | 0.0478 | 0.0446 |
| $R1$ [all data] | 0.0355 | 0.0332 |
| w$R2$ [$I > 2\sigma(I)$] | 0.0725 | 0.0749 |
| w$R2$ [all data] | 0.0821 | 0.0855 |
| CCDC | 1 994 616 | 1 994 615 |

nanostructures of several binary phases of palladium telluride using easy methods involving deployment of SSPs and controlling the compositions as well as physicochemical properties of NPs simply by using tailor-made organotellurium compounds. Additionally, it is also a promising beginning for applications of new alloy ($Pd_9Te_4$) in the field of catalysis followed by other fields such as electrocatalysis, oxygen reduction reactions, *etc.*

# Results and discussion

### Syntheses and characterization

The **L2**, **1** and **2** have been prepared (Scheme 1) and characterized with $^1$H, $^{13}$C and $^{125}$Te NMR spectroscopy (ESI: Fig. S1–S8†) and mass spectrometry (ESI: Fig. S9 and S10†). Molecular structures of **1** and **2** have also been authenticated (Fig. 1 and 2) using single crystal X-ray diffraction studies. $^{125}$Te nuclei are NMR active and very sensitive to their local electronic environment. A minor change in such an environment leads to significant changes in chemical shift positions in $^{125}$Te NMR spectroscopy. Similar phenomenon is observed with chemical shift position of the signal of free ligand **L2**. This signal undergoes a deshielding of 864 ppm when **L2** is transformed into complex **2**. It happens due to decrease in electron density

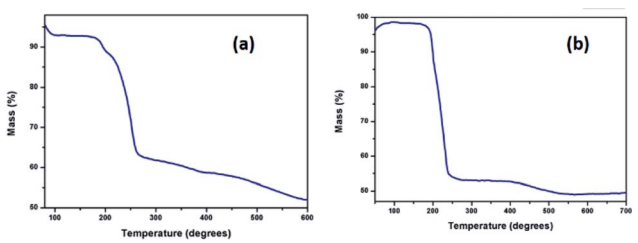


Fig. 3 TGA curves of (a) complex **1** (b) complex **2**.

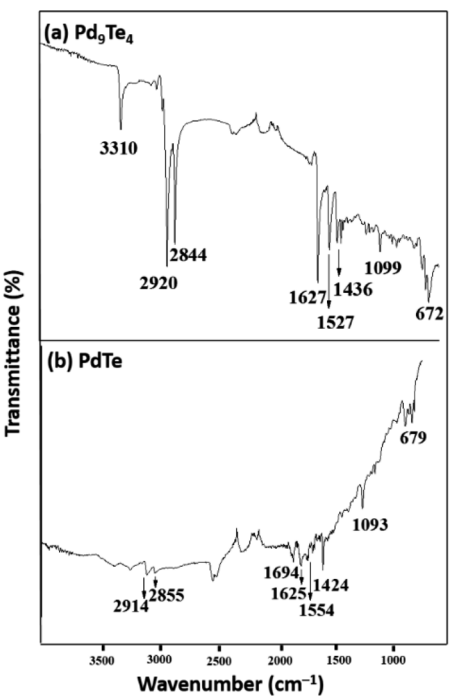


Fig. 4 FTIR spectra of (a) $Pd_9Te_4$ (b) PdTe nanostructures.

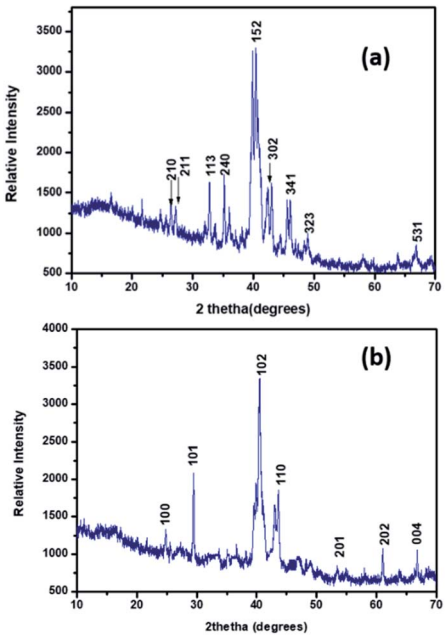


Fig. 5 PXRD spectra of (a) $Pd_9Te_4$ (b) PdTe nanostructures.

around nucleus of Te by virtue of the involvement of tellurium in the formation of a coordination bond with palladium. Single crystal X-ray diffraction studies also revealed the existence of such a bond between Te and Pd in complex **1** as well as **2**. Both the complexes exhibit a square planar geometry (Table 1) around the palladium centre. The ligand binds in a bidentate mode in **1** (Fig. 1) and tridentate mode in **2** (Fig. 2). In complex **2**, the Pd–Cl bond (*trans* to nitrogen donor) is slightly longer [2.3271(11) Å] than the one [2.3142(16) Å] in complex **1**. This Pd–Cl bond length in the **1** is consistent with the literature reports.[34] The Pd–Te bond length in both the complexes are similar *i.e.* 2.5057(6) and 2.5002(4) Å in complexes **1** and **2** respectively. The Pd–O bond length in complex **2** is 2.007(3) Å. These bond lengths are in agreement with the earlier reports.[35,36] The $C_{aryl}$–Te bond length [2.118(6) Å] is slightly shorter than $C_{alkyl}$–Te bond length [2.149(6) Å].[35,36]

Before subjecting complexes **1** and **2** to thermolysis, their thermal decomposition temperatures have been determined using thermogravimetric analysis. Such a decomposition occurred at 260 °C in case of complex **1**, and at 240 °C in case of **2**, with a weight loss of 30% and 50% respectively [Fig. 3(a) and (b)]. Hence, both the complexes were used as new single source precursors (SSP) and pyrolyzed (Scheme 1) at 260 °C and 240 °C in a mixture (1 : 1) of oleyl amine and oleic acid. This led to the formation of nanostructures of $Pd_9Te_4$ (from complex **1**) and PdTe (from complex **2**). The nanostructures have been characterized by FTIR, PXRD, SEM-EDX, TEM, DLS, BET and XPS techniques. In the FTIR spectra, the bands due to the presence of stabilizer molecules of oleyl amine and oleic acid are visible in case of both the nanostructures. The IR spectrum of $Pd_9Te_4$ [Fig. 4(a)] exhibits absorption bands at 2920 and 2844 $cm^{-1}$ due to symmetric and asymmetric stretching vibrations of the aliphatic $-CH_2$ group. Similar bands are observed at 2914 and

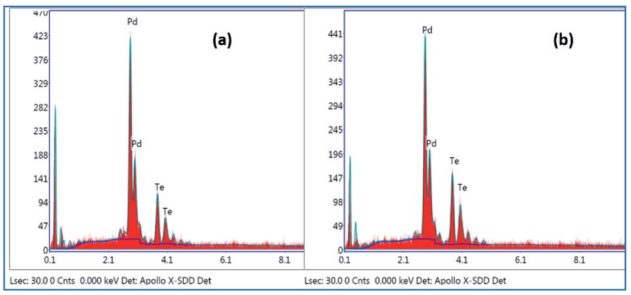


Fig. 6 SEM-EDS spectra of (a) $Pd_9Te_4$ (b) PdTe nanostructures.

2855 $cm^{-1}$ in PdTe [Fig. 3(b)]. The bands at 1627 and 1694 $cm^{-1}$ in $Pd_9Te_4$ and PdTe may be attributed to the C=O vibrations. $NH_2$ bending vibrations [Fig. 4(a) and (b)] are likely to be represented by the bands at 1527 $cm^{-1}$ in $Pd_9Te_4$ and 1554 $cm^{-1}$ in PdTe. The absorption bands at 1436, 1099 and 672 $cm^{-1}$ are likely to correspond bending vibrations of $CH_3$, C–N and C–C bonds respectively.[37,38]

The PXRD pattern of $Pd_9Te_4$ [Fig. 5(a)] reveals a monoclinic structure when matched with standard phases (JCPDS # 34-1359). The PXRD pattern of NPs **2** [Fig. 5(b)] corroborates the presence of a hexagonal PdTe phase (JCPDS # 29-0971). PXRD patterns are sharp. Such patterns do not indicate presence of any impurity as any high intensity peaks which do not belong to the phase of the material are absent. The results of the SEM-EDX studies [Fig. 6(a) and (b)] are in good agreement with the data obtained from the PXRD pattern.

The morphologies of both the nanostructures have been studied using High Resolution Transmission Electron Microscopy (HRTEM) (Fig. 7). Theses nanostructures of $Pd_9Te_4$ and PdTe (obtained from complexes **1** and **2**) appear to be spherical in shape. HRTEM images also corroborate uniform distribution of nanoparticles with size of 10–25 nm in both the cases.

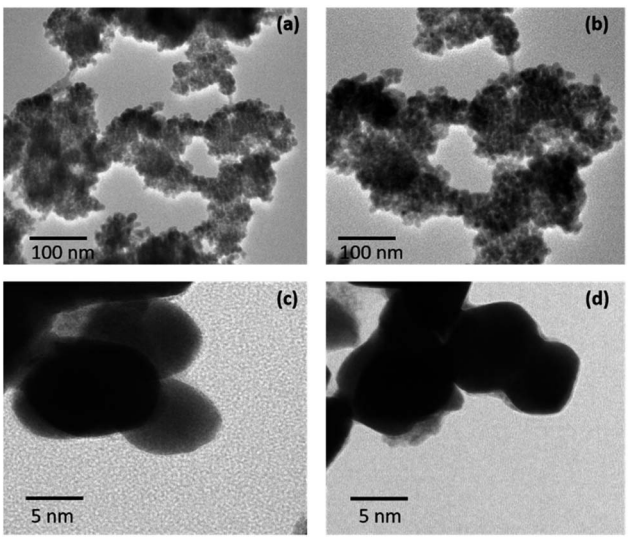


Fig. 7 HRTEM images of nanostructures of $Pd_9Te_4$ (a and c) and PdTe (b and d).

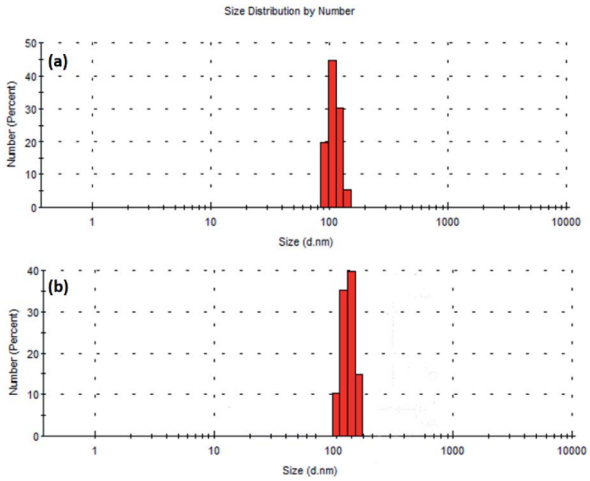


Fig. 8 DLS analysis of (a) $Pd_9Te_4$ and (b) PdTe nanostructures.

Dynamic light scattering (DLS) studies have also been performed in order to understand the particle size distribution. During such studies, the particles moves with the added solvent or stabilizer. It is well known that DLS provides information about hydrodynamic diameter (diameter of particle with hydration shell).[39,40] This diameter corresponds to the collective form of particle and stabilizer or solvent. In the present study, the hydrodynamic diameter has been found to be 106 and 220 nm for $Pd_9Te_4$ and PdTe NPs [Fig. 8(a) and (b)]. However, the molecules of the stabilizers (oleyl amine and oleic acid) are not diagnosed in the HRTEM studies as they are electron transparent. The presence of molecules of oleyl amine and oleic acid (that act as stabilizers) in the hydration shell is the most probable reason for the difference in the size, revealed by the two techniques HRTEM and DLS.[41] The value of polydispersity index (PDI) has been found to be 0.336 (below 0.5) suggesting the high colloidal stability and low sedimentation potential. It is also known from Rayleigh's approximation that the intensity of the scattering of particles is proportional to the sixth power of the diameter *i.e.* $I = d^6$. Therefore, the DLS results are influenced by the presence of larger particles even if they are very less in number (Table 2).[40]

The XPS spectral information has been used to elucidate the valence distribution of palladium (Fig. 9) and tellurium (ESI: Fig. S13 and S14†) atoms. The binding energies of both Pd-3d region and Te-3d region are given in Table S3.† Analysis of high-resolution spectrum in the binding energy region of Pd-3d in $Pd_9Te_4$ (Fig. 9) shows the presence of two sets of peaks in the Pd-3d region (336.06 eV, 341.39 eV and 337.80, 343.08 eV). The

Table 2 Particle size distribution of $Pd_9Te_4$ and PdTe nanostructures

| | | | | |
|---|---|---|---|---|
| $Pd_9Te_4$ nanostructures | | | | |
| Size (d. nm) | 91.3 | 106 | 122 | 142.5 |
| Intensity (%) | 19.7 | 44.7 | 30.3 | 5.3 |
| PdTe nanostructures | | | | |
| Size (d. nm) | 112.5 | 150 | 220 | 295.5 |
| Intensity(%) | 10.3 | 35.3 | 39.7 | 14.7 |

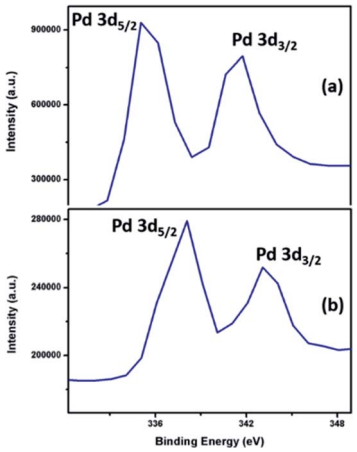


Fig. 9 XPS spectra of (a) $Pd_9Te_4$ and (b) PdTe nanostructures.

enlarged spectra of PdTe (Fig. 9) also indicated the Pd-3d peaks in the similar binding energy region (337.80 eV and 343.08 eV).

The positive shift in both the cases is attributed to the higher donation of electrons from Te to Pd centre in PdTe. Interestingly, there is a drift towards Pd(0) values as the palladium content in the phase is increased (from PdTe to $Pd_9Te_4$). The 3d spectra of Te (Fig. S14†) also reflect a doublet corresponding to $3d_{5/2}$ and $3d_{3/2}$ in $Pd_9Te_4$ (573.60 and 582.50 eV) and PdTe (374.29 eV and 583.10). Hence, the presence of both Pd(0) and Pd(II) species on the surface of both the nanostructures is indicated (details in ESI†). The surface area and pore volume were also calculated using $N_2$ adsorption–desorption insotherm (Fig. 10). The BET surface areas have been found to be 18.424 $m^2\ g^{-1}$ and 4.9565 $m^2\ g^{-1}$ for $Pd_9Te_4$ and PdTe nanostructures respectively. The average pore size was found to be less than 2 nm in both the cases, suggesting the presence of only micropores. The pore volume was calculated and found to be 0.033 and 0.008 $cm^3\ g^{-1}$ indicating that these are non-porous materials. These materials exhibit a type IV hysteresis loop that is observed when the substances have micropores and mesopores.[42]

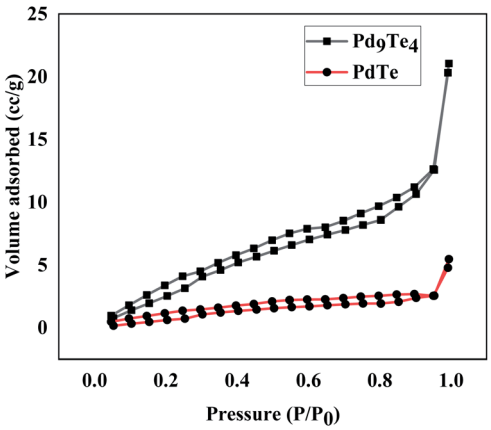


Fig. 10 $N_2$ adsorption–desorption isotherm of $Pd_9Te_4$ and PdTe nanostructures.

### Catalytic studies

The catalytic potential of both the nanostructures has been evaluated (Table 3) for Suzuki Miyaura C–C coupling (Scheme 1) of chloroarenes. These substrates were chosen for the study because aryl chlorides have easy availability. In addition, they suffer from the lowest reactivity among haloarenes (ArI, ArBr and ArCl). In case of coupling of such substrates, the palladium-based catalysts must be able to overcome the high activation barriers of the substrates. Hence, presence of electron rich active sites is desired in most homogeneous palladium catalysts. Such sites are generated by the presence of electron-donating ligands. However, the use of palladium complexes and ligands is generally avoided in chemical industry due to their high cost and toxicity. In contrast, heterogeneous catalysts, which offer the advantage of their facile reusability and compatibility with flow systems, are preferred. In such catalytic systems, high activity and stability require negatively charged or electron rich Pd species with negligible metal leaching or clustering. In this context, in recent past, nanosized bimetallic alloys have attracted attention of the researchers as they show improved catalytic activity than monometallic catalysts, at nanoscale, due to the electronic and geometrical modifications which arise as a consequence of synergic cooperation between the two metals of alloys.[43–50] In the present study, both $Pd_9Te_4$ and PdTe are bimetallic alloys in which active Pd atoms are incorporated in a lattice together with Te.[25,26] Hence, these intermetallic phases are likely to offer the advantage of hosting solid active sites. In addition, $Pd_9Te_4$ has a higher valence electron concentration[26] which may play a role in generating electron rich palladium species.

Before conducting catalytic studies on the nanosized PdTe and $Pd_9Te_4$, reaction conditions and parameters were optimized. Such parameters include use of $K_2CO_3$ as a base, and aqueous DMF (DMF : Water = 1 : 1) (ESI: Table S4,† entry 2) as solvent system.

Coupling reactions of all the aryl chlorides (*i.e.* 4-chlorobenzaldehyde, 4-chloronitrobenzene, 4-chloroacetophenone, 4-chlorobenzonitrile and chlorobenzene) were carried out and studied at these optimized reaction conditions. All the substrates gave comparable yields of cross-coupled products. 4-Chlorobenzaldehyde was converted to 4-biphenylcarboxaldehyde in 88% and 87% conversion when NPs of $Pd_9Te_4$ and PdTe (5.0 mg) were used as a catalyst in 12 hours (Table 3, entry 1). The conversion of the substrates into the products, observed in the reactions of 4-chloronitrobenzene and 4-chlorobenzonitrile, were 85% when $Pd_9Te_4$ was used as a catalyst (Table 3, entry 2, 4). However, when nanocatalyst PdTe was employed, a marginally decrease was observed, and % conversions were found to be 83% and 84% respectively (Table 3, entry 2, 4). Other substrates (*i.e.* 4-chloroacetophenone and chlorobenzene) also gave good (*i.e.* $\geq$78%) conversions. Hence, it may be inferred that nanoparticles of palladium rich phase $Pd_9Te_4$ are slightly more efficient than those of PdTe.

Table 3 Results of catalysis Suzuki coupling between aryl chlorides and phenylboronic acid by nanostructures of $Pd_9Te_4$ and PdTe[a]

| S. no | Substrate | % conversion (**NPs 1**) | % conversion (**NPs 2**) |
|---|---|---|---|
| [1] | 4-Chlorobenzaldehyde | 88 | 87 |
| [2] | 4-Chloronitrobenzene | 85 | 83 |
| [3] | 4-Chloroacetophenone | 79 | 78 |
| [4] | 4-Chlorobenzonitrile | 85 | 84 |
| [5] | Chlorobenzene | 82 | 80 |

[a] Reaction conditions: aryl chloride (1.0 mmol), phenylboronic acid (1.1 mmol), $K_2CO_3$ (2.0 mmol), catalyst 5.0 mg, time 12 h, temperature 100 °C.

The number of catalytic systems in general and nanocatalytic systems in particular, which are competent to catalyze the coupling of aryl chlorides, is not very high.[51–63] In fact, aryl chlorides are the least reactive substrates, and most of the catalytic systems either show inactivity for these substrates or show very low efficiency. Many of the reported palladium based nanocatalytic systems require longer reaction times (Table 4, entry 2, 4)[53,55] and/or give lower conversions (Table 4, entry 1, 3, 15)[52,54,63] in comparison to our $Pd_9Te_4$ and PdTe nanocatalysts. However, some of them are able to operate in EtOH/$H_2O$ (Table 4, entry 1–4, 15).[52–55,63]

Reports about the use of nanosized alloys of palladium as catalysts of Suzuki coupling are rare, but not non-existent in the literature. Such alloys include $Pd_1Ni_4$, CuPd, $Y_3Pd_2$, $Pd_3Te_2$ and $Pd_{17}Se_{15}$.[43,48,52,57,64] The alloy $Pd_1Ni_4$ has been grafted on carbon nanofibers and the resulting system ($Pd_1Ni_4$/CNF) gives only 7% conversion in the reaction of phenylboronic acid and chlorobenzaldehyde after 5 hours at 80 °C using 5 mg of the catalyst (Table 4, entry 1).[52] Its performance is insignificant in comparison to that of palladium telluride alloys in the present study. $Pd_3Te_2$ is one of those rarest of the rare palladium telluride alloys which have been used to catalyse Suzuki coupling.[57] It has been employed to convert bromoarenes into their respective products at 2–3 mol% catalyst loading (Table 4, entry 6).[57] Its application in the catalysis of aryl chlorides is not reported. The efficiencies of $Pd_9Te_4$ and PdTe nanostructures are also better than those of some nanosized binary phases of palladium sulphides (PdS and $Pd_{16}S_7$) in catalyzing coupling reactions of chlorobenzene (Table 4, entry 11, 12).[61] The nanosized $Pd_{16}S_7$, which is generated *in situ* during the course of a Suzuki reaction using the palladacycle of a thioether ligand as a catalyst, has been isolated and tested independently as a catalyst. Such $Pd_{16}S_7$ nanoparticles catalyze the coupling of only aryl bromides (Table 4, entry 13 and 14) and that too at a high loading.[62]

In the recent past, organosulphur and organoselenium compounds have been used as stabilizers to obtain uniformly dispersed catalytically active nanoparticles of palladium(0) for Suzuki coupling.[58–60] On assessing their performance on various parameters (such as reaction time, catalyst loading and % conversions), it becomes clear that these are less efficient[58–60] than the present nanocatalytic systems (*i.e.* $Pd_9Te_4$ and PdTe). The Pd(0) nanoparticles (stabilized with bulky organosulphur ligand) catalyze the coupling of chlorobenzene with phenylboronic acid and give much lesser conversion (~45%) at 100 °C (Table 4, entry 7).[58] In another similar study, Pd(0) nanoparticles (stabilized by anthracene based-organosulphur ligand) have been used to catalyse the coupling of 4-chlorobenzaldehyde (not

Table 4 Performance of known palladium based nanocatalytic systems for Suzuki coupling between chlorobenzene and $PhB(OH)_2$

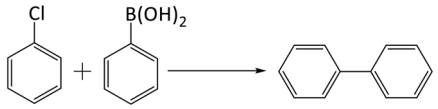


| Entry no. | Catalyst | Solvent | Catalyst amount | Time (h) | Temp (°) | % conversion | Ref. |
|---|---|---|---|---|---|---|---|
| [1] | $Pd_1Ni_4$/CNF | EtOH/$H_2O$ | 5 mg | 5 | 80 | 7 | 52 |
| [2] | Isoniazide-MWCNTs-Pd | EtOH/$H_2O$ | 14 mg | 24 | 60 | 70 | 53 |
| [3] | Chitosan-biguanidine/Pd | EtOH/$H_2O$ | 10 mg | 10 | 40 | 70 | 54 |
| [4] | MWCNTs/CC-SH/Pd | EtOH/$H_2O$ | 10 mg | 24 | 80 | 70 | 55 |
| [5] | Pd NPs@$PPh_2$-$SiO_2$ | DMF | 0.5 mol% | 5 | 100 | 95 | 56 |
| [6][a] | $Pd_3Te_2$ | Aq. DMF | 2 mol% | 15 | 100 | 86 | 57 |
| [7] | Pd(0) NPs (stabilized by bulky organosulphur ligand) | Aq. DMF | 3 mg | 3 | 100 | 45 | 58 |
| [8][b] | Pd(0) NPs (stabilized by anthracene-based organosulphur ligand) | Aq. DMF | 5 mg | 12 | 100 | 75 | 59 |
| [9][b] | Pd(0) NPs (stabilized with anthracene based organoselenium ligand) | Aq. DMF | 5 mg | 12 | 100 | 84 | 59 |
| [10][b] | Pd(0) NPs (stabilized with didocosyl selenide) | Aq. DMF | 5 mol% | 24 | 100 | 32 | 60 |
| [11] | PdS | Aq. DMF | 5 mg | 12 | 90 | 78 | 61 |
| [12] | $Pd_{16}S_7$ | Aq. DMF | 5 mg | 12 | 90 | 74 | 61 |
| [13][c] | $Pd_{16}S_7$ | Aq. DMF | 0.1 mol% | 24 | 100 | 88 | 62 |
| [14][c] | $Pd_{16}S_7$ | Aq. DMF | 0.1 mol% | 24 | 100 | 81 | 62 |
| [15] | Pd@AGPO | EtOH/$H_2O$ | 5 mg | 6 | 80 | 25 | 63 |
| [16] | $Pd_9Te_4$ | Aq. DMF | 5 mg | 12 | 100 | 84 | Present work |
| [17] | PdTe | Aq. DMF | 5 mg | 12 | 100 | 82 | Present work |

[a] 4-Bromobenzaldehyde. [b] 4-Chlorobenzaldehyde. [c] 1-Bromo-4-nitrobenzene.

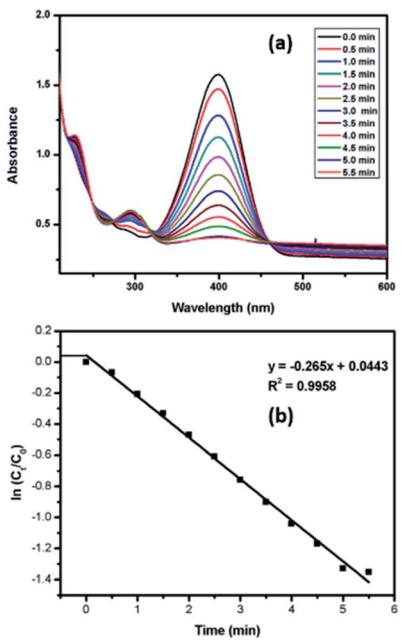


Fig. 11 (a) Reduction of 4-nitrophenol (b) plot of $\ln(C_t/C_0)$ *versus* time: determination of rate constant.

chlorobenzene) with phenylboronic acid[59] and only 75% conversion (Table 4, entry 8) was noticed. It is lower than that observed with $Pd_9Te_4$ and PdTe nanocatalysts. However, when anthracene-based organoselenium ligand is used as a stabilizer, similar Pd(0) nanoparticles give better conversions (Table 4, entry 9)[59] which is equivalent to those obtained in the present study. Pd(0) nanoparticles, stabilized by didocosyl selenide (*i.e.* $C_{22}H_{45}$–Se–$C_{22}H_{45}$) also show significantly lower efficiency and give only 32% conversion in the catalysis of coupling of 4-chlorobenzaldehyde (Table 4, entry 10).[60]

Hence, it is inferred that the present palladium telluride alloys have appreciably significant catalytic potential for catalysis of Suzuki coupling of aryl chlorides, the most difficult and unreactive substrates among aryl halides, and also have an edge over the many of the reported catalytic systems either in terms of reaction time, the % conversion or recyclability.

The catalytic potential of nanoparticles of both $Pd_9Te_4$ and PdTe has also been investigated for the reduction of nitroarenes. For exploring the possibility of catalytic use in water, 4-nitrophenol (a listed carcinogen pollutant) was chosen as substrate. Both the nanostructures catalyzed the reaction completely within 5.5 minutes. The kinetic studies for 4-nitrophenol reduction (Scheme 1) using PdTe nanostructures (**NPs 2**)

Table 5 Performance of known palladium based nanocatalytic systems for reduction of 4-nitrophenol in aqueous solution at room temperature

| Entry no. | Catalyst | Time (min) | Rate constant ($min^{-1}$) | Ref. |
|---|---|---|---|---|
| [1] | Pd-FG | 12 | 0.141 | 65 |
| [2] | $Fe_3O_4$@TA/Pd NPs | 4 | 1.1 | 66 |
| [3] | Pd(II) complex on GO-$MnFe_2O_4$ | 4 | 0.72 | 67 |
| [4] | Pd-CS/PEO/IA catalyst | 30 | 0.114 | 68 |
| [5] | Au/Ag/Pd trimetallic NPs | 20 | 0.0466 | 69 |
| [6] | $Pd_9Te_4$ | 5.5 | 0.265 | Present study |
| [7] | PdTe | 5.5 | 0.265 | Present study |

have been carried out using UV-Vis spectroscopy. It was observed that a bathochromic shift appeared in the spectrum when $NaBH_4$ was added because of the formation of the phenolate ion and absorption frequency ($\lambda_{max}$) shifts to 400 nm.

The absorption at $\lambda_{max} = 400$ nm decreased with respect to time and two new bands appeared at 226 nm and 300 nm respectively [Fig. 11(a)] because of the formation of 4-aminophenol. The reaction was monitored until the band at 400 nm completely disappeared. The rate constant for the reaction has also been determined by plotting a graph of ln $C_t/C_0$ *vs.* time [Fig. 11(b)]. In this graph, there are two portions labelled ab and bc. Portion ab has very little slope and represents the induction time or the delay in the start of the reaction.

It occurs when the substrate takes some time to adsorb on the catalytic surface.[30] The portion bc has higher slope values and gives the rate constant '*K*' for the reaction. In the present work, the novel palladium-based catalyst shows high rate constant of 0.265 $min^{-1}$.

For this reduction reaction too, the present alloy nanostructures are more efficient than many of the known palladium based nanocatalysts (Table 5, entry 1, 4, 5)[65,68,69] in terms of rate constant. However, some heterogeneous palladium-based catalysts (immobilized on the solid support) are known to show a better rate constant (Table 5, entry 2, 3).[66,67]

### Recyclability of nano-catalysts

The recyclability studies have also been carried out using $Pd_9Te_4$ nanostructures for Suzuki Miyaura C–C coupling reaction between 4-chlorobenzaldehyde and phenylboronic acid at 100 °C in aqueous DMF in the presence of $Pd_9Te_4$ (**NPs 1**) as catalyst. The alloy nanoparticles have been found to be recyclable upto six reaction cycles with some loss in the catalytic activity. The nanocatalysts show a slight decrease after every reaction cycle. Conversion is 88% in the first cycle, 87% in second cycle, 80% in the third cycle, 78% in fourth cycle, 75% in fifth cycle and 68% in the sixth cycle. A decrease of around 20% in the conversion of the substrate into the coupled product is observed in the sixth catalytic reaction cycle (conversion = 68%) in comparison to the first reaction cycle (conversion = 88%) (Fig. 12). Hence, it implies that the present alloy nanoparticles are recyclable and can be employed repeatedly in many reaction cycles. Therefore, this alloy may increase the economy of the catalytic process if used as a catalyst.

## Experimental section

### Physical measurements

$^1H$, $^{13}C\{^1H\}$ NMR was carried out on 300 MHz Bruker Spectrospin DPX-300 NMR spectrophotometer at 300.13 and 75.47 MHz respectively. $^{125}Te\{^1H\}$ NMR was performed on Bruker Advance III 500 MHz Spectrometer at SAIF, IIT Madras. Single crystal X-ray diffraction studies were performed on Supernova X-ray diffractometer system at 150 K using Mo Kα radiation (0.710 Å). CrysalisPro Software (online version) was used for data collection. The structure was solved by direct methods using olex2, SHELXS-97 and refined by full matrix least-squares with SHELXL-97, refining on F2. The image was created using the program diamond. High resolution mass spectrometry (HRMS) was carried out Bruker High Impact HD spectrometer by taking the sample in acetonitrile. Powder X-ray diffraction (PXRD) studies were carried out on Panalytical X'Pert diffractometer with Cu filtered radiation using a scan speed of 2° per min and scan step of 0.02°. The elemental composition of NPs was analysed by using an Energy Dispersive X-ray (EDX) system (Model: JSM 6100). High Resolution Transmission Electron Microscopic (HRTEM) studies were carried out with a FEI Tecnai G2-S-twin electron microscope operated at 200 kV. The specimens for HRTEM were prepared by dispersing the nanoparticles in methanol and ultrasonicating them. Then, the slurry was dropped onto a porous carbon film supported on a copper grid and dried in air. Pervac spectrophotometer was

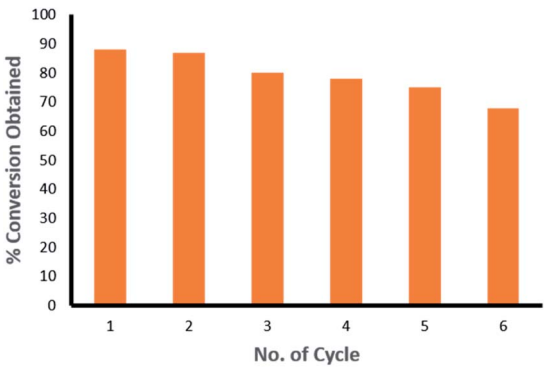


Fig. 12 Recyclability plot of catalytic use of $Pd_9Te_4$ alloy nanoparticles in the Suzuki coupling of 4-chlorobenzaldehyde and phenylboronic acid.

utilized for recording X-ray photoelectron spectroscopy (XPS) data. Dynamic Light Scattering (DLS) studies have been carried out using Malvern zetasizer nano ZSP instrument. Surface area has been analysed on autosorb IQ quantachrome instrument. The $N_2$ adsorption–desorption analysis was carried out using Bruanauer–Emmet–Teller (BET) and Barrett–Joyner–Halenda (BJH) models to get a clear picture of surface area and porosity of the nanomaterials. FTIR has been performed on Shimadzu IRSpirit spectrophotometer.

### Chemicals

Diphenyl ditelluride, 2′-hydroxyacetophenone and palladium chloride are procured from Sigma Aldrich. Solvents and other chemicals have been procured from local dealers and were used as received. **L1** were prepared according to the reported procedure.[70]

### Synthesis of L2

A solution of **L1** (0.25 g, 1.0 mmol) in ethanol was taken in an oven dried round bottom flask and stirred at room temperature. 2'-Hydroxyacetophenone (0.136 g, 1.0 mmol) was added dropwise to the reaction mixture and it was further stirred for 6 hours at room temperature under ambient conditions. The solvent was evaporated and the **L2** was dissolved in chloroform and precipitated by the addition of hexane to obtain yellow coloured solid.

**L2.** NMR: $^1$H ($CDCl_3$, TMS, 25 °C) $\delta$(ppm): 15.91 (1H, s), 7.77 (2H, d, $J = 7.5$ Hz), 7.50 (1H, d, $J = 8.0$ Hz), 7.27–7.31 (2H, m), 7.21 (2H, t, $J = 7.5.0$ Hz), 6.94 (1H, d, $J = 8.5$ Hz), 6.78 (1H, t, $J = 8.0$ Hz), 3.94 (2H, t, $J = 7.0$ Hz), 3.20 (2H, t, $J = 7.5$ Hz), 2.26 (3H, s). $^{13}$C{$^1$H} ($CDCl_3$, TMS, 25 °C) $\delta$(ppm): 171.82, 163.48, 138.83, 137.56, 132.39, 129.32, 128.07, 127.95, 119.34, 118.73, 117.25, 110.93, 51.13, 14.48, 8.77. $^{125}$Te {$^1$H} ($CDCl_3$, $Me_2Te_2$, 25 °C) $\delta$ (ppm): 467.73.

### Synthesis of 1/2

A mixture of **L1**/**L2** (0.1 mmol) and $Pd(CH_3CN)_2Cl_2$ (0.026 g, 0.1 mmol) was taken in chloroform and stirred at room temperature for 15 minutes at room temperature. The Pd(II) complex was precipitated with the addition of hexane, filtered and dried.

**1.** Yield (0.0367, 86%), NMR: $^1$H ($CDCl_3$, TMS, 25 °C) $\delta$ (ppm): 8.05 (2H, d, $J = 6.0$ Hz), 7.37 (2H, m), 7.19 (1H, m), 1.94 (2H, t, $J = 7.0$ Hz), 1.16 (2H, t, $J = 12.0$ Hz). $^{125}$Te{$^1$H} ($CDCl_3$, $Me_2Te_2$, 25 °C) $\delta$(ppm): 1470.69. HRMS ($CH_3CN$): $[M - Cl^-]^+$ $m/z$ calcd for $[C_8H_{11}ClNPdTe]^+$ 391.8777; found 391.8766 ($\Delta = 2.8\%$).

**2.** Yield (0.0437, 80%), NMR: $^1$H ($CDCl_3$, TMS, 25 °C) $\delta$(ppm): 12.09 (1H, s), 7.98 (2H, t, $J = 6.0$ Hz), 7.60 (1H, m), 7.32–7.35 (3H, m), 7.23–7.25 (1H, m), 6.73–6.81 (2H, m), 2.40 (3H, s), 2.33 (4H, m). $^{125}$Te{$^1$H} ($CDCl_3$, $Me_2Te_2$, 25 °C) $\delta$(ppm): 1331.70. HRMS ($CH_3CN$): $[M + Na]^+$ $m/z$ calcd for $[C_{16}H_{16}ClNOPdTeNa]^+$ 531.9017; found 531.9004 ($\Delta = 2.4\%$).

### Procedure for the development of $Pd_9Te_4$ and PdTe nanostructures from Pd(II) complexes 1 and 2

An oven dried three necked flask was purged with nitrogen before the addition of the reactants. 0.5 mmol (0.213 g/0.253 g) of the Pd(II) complex (**1**/**2**) was added alongwith 10 mL of oleic acid–oleyl amine solution (5 mL/5 mL). The mixture was heated to 260 °C in case of **1** and 240 °C in case of **2** under $N_2$ with continuous stirring for 2 hours. The colour of the complexes changed from yellow/orange to dark brown within the first 30 minutes and the black precipitate started to form eventually. Thereafter, mixture was cooled to room temperature and acetone (20 mL) was added to isolate the black precipitate which was further separated by centrifugation. The isolated precipitate was washed several times with methanol (20 mL) and dried *in vacuo*.

### Procedure for Suzuki Miyaura coupling reaction of chloroarenes

An oven dried round bottom flask was discharged with chloroarene (1.0 mmol), phenyl boronic acid (1.1 mmol), $K_2CO_3$ (2.0 mmol), catalyst (5.0 mg) in aqueous DMF (DMF : Water = 4 : 1). The reaction mixture was refluxed for 12 hours at 100 °C. After the requisite time, the reaction was cooled and quenched with water. The product was extracted with diethyl ether and dried over anhydrous sodium sulphate. The solvent was evaporated on rotary evaporator. The yield of the product was estimated using $^1$H NMR spectroscopy.

### Procedure for catalytic reduction of nitroarenes

The kinetic studies ascertained to the reduction of 4-nitrophenol have been carried out in quartz cuvettes of path length 1 cm and utilizing a total aqueous volume of 1.0 mL. For each test, a known volume of the catalyst *i.e.* 10 μL was pipetted out from a stock solution (1.0 mg NPs of **1**/**2** dispersed in 1.0 mL) in cuvette. To this, 1.0 mL of $10^{-4}$ M aqueous solution of 4-nitrophenol was added. Just before the placement of the cuvette in the spectrophotometer, $NaBH_4$ was added. The addition of $NaBH_4$ intensified the colour leading to a bathochromic shift. The absorption spectrum was recorded in the range of 200–800 nm.

### Catalytic recyclability

An oven-dried round bottom flask was charged with 4-chlorobenzaldehyde (1.0 mmol, 0.140 g), phenylboronic acid (1.1 mmol, 0.133 g), $K_2CO_3$ (2.0 mmol, 0.276 g) and aqueous DMF (DMF : Water = 4 : 1). Nanoparticles (5 mg of **NPs 1**), were added to the reaction mixture and the temperature was maintained at 100 °C. The progress of the reaction was monitored with TLC. After completion of the reaction, water and ethyl acetate were added and the mixture was centrifuged. The black residue (*i.e.* nanocatalysts) was collected and washed with methanol in order to remove the organic content and base. The nanocatalysts were dried *in vacuo*. The organic layer from water–ethyl acetate was separated and the solvent was evaporated off. The residue was subjected to $^1$H NMR for conversion estimation. The NPs separated were reused for the next cycle and this procedure was repeated for six times.

## Conclusions

The present work involves first study not only on the precursor-architecture controlled synthesis of intermetallic binary phase PdTe and $Pd_9Te_4$ nanostructures *via* single source precursor route but also on their catalytic potential for Suzuki coupling and reduction of nitrophenol. The Pd(II) complexes **1** and **2** of different organotellurium ligands have a major structural difference in terms of coordination mode of the ligand *i.e.* bidentate in case of **1** and tridentate in case of **2**. They function as designers SSPs while undergoing thermolysis under similar conditions and lead to the formation of nanoparticles of different bimetallic alloy materials ($Pd_9Te_4$ in case of **1** and PdTe in case of **2**). Molecular precursor's architecture controls the composition of the product *i.e.* nanomaterial. Both the nanostructures do not agglomerate and show uniformity in dispersion. These appear to be spherical in shape. Catalytic studies reveal that nanostructures of both the alloys have catalytic potential for Suzuki–Miyaura C–C coupling of aryl chlorides (the most difficult and unreactive substrates) and reduction of 4-nitrophenol. The nanocatalysts are also reusable upto six reaction cycles, explored in case of Suzuki coupling. The results of this report open a field for development of nanostructures of several binary phases of palladium telluride using easy methods involving single source precursor route. In addition, applications of such nanosized binary phase of Pd–Te alloys will be open for exploration in various fields including catalysis, electrocatalysis, oxygen reduction reactions for use in magnesium air batteries, development of electrodes, *etc.*

## Conflicts of interest

There are no conflicts to declare.

## Acknowledgements

AA and AK would like to acknowledge Department of Science and Technology, Science and Engineering Research Board (DST SERB) [Project: ECR/2016/001549] for fellowship and financial assistance. Financial assistance provided by UGC under its UGC-BSR Research Start-Up-Grant [No. F.30-371/2017/(BSR) Dated 10 July 2017] is also acknowledged. PO also acknowledges DST for INSPIRE Fellowship [No. DST/INSPIRE Fellowship/2017/IF170491]. SK thanks DST for INSPIRE Faculty Award [DST/INSPIRE/04/2015/002971]. Authors acknowledge SAIF Facility, I.I.T. Madras for $^{125}$Te NMR.

## Notes and references

1 L. Polavarapu, S. Mourdikoudis, I. P. Santos and J. P. Juste, *CrystEngComm*, 2015, **17**, 3727.
2 D. Jamwal and S. K. Mehta, *ChemistrySelect*, 2019, **4**, 1943.
3 J. Zhitong, M. Zhang, M. Wang, C. Feng and Z.-S. Wang, *Acc. Chem. Res.*, 2017, **50**, 895.
4 J. D. Major, R. E. Treharne, L. J. Phillips and K. Durose, *Nature*, 2014, **511**, 334.
5 Q. Huang, F. Dang, H. Zhu, L. Zhao, B. He, Y. Wang, J. Wang and X. J. Mai, *J. Power Sources*, 2020, **451**, 227738.
6 V. K. Jain and G. Kedarnath, *Phys. Sci. Rev.*, 2018, **4**, 20170127.
7 M. D. Khan, M. A. Malik and N. Revaprasadu, *Coord. Chem. Rev.*, 2019, **388**, 24.
8 V. K. Jain and R. S. Chauhan, *Coord. Chem. Rev.*, 2016, **306**, 270.
9 R. Zhao, D. Tang, L. Huan, Q. Wu, W. Li, X. Zhang, M. Chen and G. Diao, *Sol. Energy*, 2019, **178**, 241.
10 S. Kukunuri, S. N. Karthick and S. Sampath, *J. Mater. Chem. A*, 2015, **3**, 17144.
11 S. Kukunuri, K. Naik and S. Sampath, *J. Mater. Chem. A*, 2017, **5**, 4660.
12 S. Bag, I. U. Arachchige and M. G. Kanatzidis, *J. Mater. Chem.*, 2008, **18**, 3628.
13 S. C. Sarma, V. Vemuri, V. Mishra and S. C. Peter, *J. Mater. Chem. A*, 2019, **7**, 979.
14 S. Kukunuri, M. P. Austeria and S. Sampath, *Chem. Commun.*, 2016, **52**, 206.
15 S. Gupta, N. Chandna, P. Dubey, A. K. Singh and N. Jain, *Chem. Commun.*, 2018, **54**, 7511.
16 H. Joshi, K. N. Sharma, A. K. Sharma, O. Prakash and A. K. Singh, *Chem. Commun.*, 2013, **49**, 7483.
17 K. N. Sharma, H. Joshi, V. V. Singh, P. Singh and A. K. Singh, *Dalton Trans.*, 2013, **42**, 3908.
18 L. Jiao, F. Li, X. Li, R. Ren, J. Li, X. Jhou, J. Jin and R. Li, *Nanoscale*, 2015, **7**, 18441.
19 T. Komatsu, K. Inaba, T. Uezono, A. Onda and T. Yashima, *Appl. Catal., A*, 2003, **251**, 315.
20 M. Huang, F. Wang, L. Li and Y. Guo, *J. Power Sources*, 2008, **178**, 48.
21 J. Akhtar, R. F. Mehmood, M. A. Malik, N. Iqbal, P. O'Brien and J. Raftery, *Chem. Commun.*, 2011, **47**, 1899.
22 S. Dey and V. K. Jain, *Platinum Met. Rev.*, 2004, **48**, 16.
23 H. Takahashi, N. Konishi, H. Ohno, K. Takahashi, Y. Koike, K. Asakura and A. Muramatsu, *Appl. Catal., A*, 2011, **392**, 80.
24 K. Mariappan, S. J. P. Varapragasam, M. R. Hansen, S. Rasalingam, M. Alaparthi and A. G. Sykes, *J. Organomet. Chem.*, 2018, **866**, 251.
25 P. Matkovic and K. Schubert, *J. Less-Common Met.*, 1978, **58**, 39.
26 W. S. Kim and G. Y. Chao, *J. Less-Common Met.*, 1990, **162**, 61.
27 D. Kumar, H. Singh, S. Jouen, B. Hannoyer and S. Banerjee, *RSC Adv.*, 2015, **5**, 7138.
28 J. Yang, X. Wang, Y. Qu, X. Wang, H. Huo, Q. Fan, J. Wang, L. -M. Yang and Y. Wu, *Adv. Energy Mater.*, 2020, **10**, 2001709.
29 J.-H. Liu, L.-M. Yang and E. Ganz, *ACS Sustainable Chem. Eng.*, 2018, **6**, 15494.
30 J.-H. Liu, L.-M. Yang and E. Ganz, *J. Mater. Chem. A*, 2019, **7**, 3805.
31 J. J.-H. Liu, L.-M. Yang and E. Ganz, *J. Mater. Chem. A*, 2019, **7**, 11944.
32 I. P. Belestkaya, F. Alonso and V. Tyurin, *Coord. Chem. Rev.*, 2019, **385**, 137.
33 M. Orlandi, D. Brenna, R. Harms, S. Jost and M. Benaglia, *Org. Process Res. Dev.*, 2018, **22**, 430.

34 A. Arora, P. Oswal, G. K. Rao, J. Kaushal, S. Kumar, A. K. Singh and A. Kumar, *ChemistrySelect*, 2019, **4**, 10765.
35 A. Kumar, M. Agarwal and A. K. Singh, *J. Organomet. Chem.*, 2008, **69**, 3533.
36 A. Kumar, M. Agarwal, A. K. Singh and R. J. Butcher, *Inorg. Chim. Acta*, 2009, **362**, 3208.
37 N. S. Labidi and A. Iddoku, *J. Saudi Chem. Soc.*, 2007, **11**, 221.
38 F. Lan, J. Bai and H. Wang, *RSC Adv.*, 2018, **8**, 16866.
39 K. Anand, C. Tikole, A. Phulukdaree, B. Ranjan, A. Chuturgoon, S. Singh and R. M. Gengen, *Photochem. Photobiol.*, 2016, **165**, 87.
40 K. Scheurell, J. Noack, R. Konig, J. Hegmann, R. Jahn, Th. Hofmann, P. Lobmann, B. Litner, P. Gracia-Jaun, J. Eicher and E. Kemnitz, *Dalton Trans.*, 2015, **44**, 19501.
41 J. Lim, S. P. Yeap, H. X. Che and S. C. Low, *Nanoscale Res. Lett.*, 2013, **8**, 281.
42 A. V. Neimark, K. S. W. Sing and M. Thommes, *Handbook of Heterogeneous Catalysis*, Wiley-VCH Verlag GmbH & Co. KGaA, Weinheim, 2nd edn, 2008, p. 721.
43 A. Dhankhar, R. K. Rai, D. Tyagi, X. Yao and S. K. Singh, *ChemistrySelect*, 2016, **1**, 3223.
44 N. Ghanbari, S. J. Hoseini and M. Bahrami, *Ultrason. Sonochem.*, 2017, **39**, 467.
45 P. Phukan, P. R. Boruah, P. S. Gehlot, A. Kumar, A. Bordoloi and D. Sarma, *ChemistrySelect*, 2017, **2**, 11795.
46 R. K. Rai, K. Gupta, S. Behrens, J. Li, Q. Xu and S. K. Singh, *ChemCatChem*, 2015, **7**, 1806.
47 R. K. Rai, K. Gupta, D. Tyagi, A. Mahata, S. Behrens, X. Yang, Q. Xu, B. Pathaka and S. K. Singh, *Catal. Sci. Technol.*, 2016, **6**, 5567.
48 T.-N. Ye, Y. Lu, Z. Xiao, J. Li, T. Nakao, H. Abe, Y. Niwa, M. Kitano, T. Tada and H. Hosono, *Nat. Commun.*, 2019, **10**, 1.
49 V. Babel and B. L. Hiran, *Catal. Lett.*, 2020, **150**, 1865.
50 D. R. Pye and N. P. Mankad, *Chem. Sci.*, 2017, **8**, 1705.
51 A. Kumar, G. K. Rao, F. Saleem and A. K. Singh, *Dalton Trans.*, 2012, **41**, 11949.
52 G. Bao, J. Bai and C. Li, *Org. Chem. Front.*, 2019, **6**, 352.
53 M. Hajighorbani and M. Hekmati, *RSC Adv.*, 2016, **6**, 88916.
54 H. Veisi, M. Ghadermazi and A. Naderi, *Appl. Organomet. Chem.*, 2016, **30**, 341.
55 H. Veisi, A. Nikseresht, N. Ahmadi, K. Khosravi and F. Saeidifar, *Polyhedron*, 2019, **162**, 240.
56 D. Sahu and P. Das, *RSC Adv.*, 2015, **5**, 3512.
57 G. K. Rao, A. Kumar, M. P. Singh and A. K. Singh, *J. Organomet. Chem.*, 2014, **749**, 1.
58 P. Sharma, A. Arora, P. Oswal, G. K. Rao, J. Kaushal, S. Kumar, S. Kumar, M. P. Singh, A. K. Singh and A. Kumar, *Polyhedron*, 2019, **171**, 120.
59 P. Oswal, A. Arora, J. Kaushal, G. K. Rao, S. Kumar, A. K. Singh and A. Kumar, *RSC Adv.*, 2019, **9**, 22313.
60 G. K. Rao, A. Kumar, B. Kumar and A. K. Singh, *Dalton Trans.*, 2012, **41**, 4306.
61 P. Oswal, A. Arora, S. Singh, G. K. Rao, S. Kumar, A. K. Singh and A. Kumar, *Catal. Commun.*, 2021, **149**, 106242.
62 G. K. Rao, A. Kumar, S. Kumar, U. B. Dupare and A. K. Singh, *Organometallics*, 2013, **32**, 2452.
63 V. B. Saptal, M. V. Saptal, R. S. Mane, T. Sasaki and B. M. Bhanage, *ACS Omega*, 2019, **4**, 643.
64 Z. Wang, C. Xu, G. Gao and X. Li, *RSC Adv.*, 2014, **4**, 13644.
65 G. K. Rao, A. Kumar, J. Ahmed and A. K. Singh, *Chem. Commun.*, 2010, **46**, 5954.
66 H. Veisi, M. Pirhayati, A. Kakanejadifard, P. Mohammadi, M. R. Abdi, J. Gholami and S. Hemmati, *ChemistrySelect*, 2018, **3**, 1820.
67 K. Karami and N. S. Mousavi, *Dalton Trans.*, 2018, **47**, 4175.
68 L. Liang, L. Nie, M. Jiang, F. Bie, L. Shao, C. Qi, X. M. Zhang and X. Liu, *New J. Chem.*, 2018, **42**, 11023.
69 K. Suwannarat, K. Thongthai, S. Ananta and L. Srisombat, *J. Colloid Interface Sci.*, 2018, **540**, 73.
70 J. Zakrzewski, B. Huras, A. Kietczewska and M. Krawczyk, *RSC Adv.*, 2016, **6**, 98829.